NUCL SCI TECH (2020) 31:12
https://doi.org/10.1007/s41365-019-0715-y

Simulation of gamma minitype reference radiation for calibration of personal dosimeter

Yi-Xin Liu[1,2] · Yi-Kun Qian[2,3] · Zhi-Qiang Chen[1] · Biao Wei[3] · Peng Feng[3] · Ben-Jiang Mao[2]

Received: 16 July 2019 / Revised: 31 October 2019 / Accepted: 5 November 2019 / Published online: 3 January 2020

Abstract An investigation using Monte Carlo simulation on a minitype reference radiation (MRR) for the calibration of gamma personal dosimeters is reported. The distributions of dose rate and scattering gamma spectrum are the main simulation objects with the variable physical structures of MRR and the dosimeters as parameters that are to be calibrated. Further, the influences on the reference radiation caused by these parameters are analyzed in detail. This work provides a theoretical basis for better understanding of MRR used for calibration of gamma personal dosimeters. This analysis can help in the development of a calibration technology for such tools based on MRR.

Keywords Gamma personal dosimeter · Minitype reference radiation · Monte Carlo simulation · Calibration

This work was supported by the National Natural Science Foundation of China (Nos. 11805111 and 11525521) and the Fundamental Research Funds for the Central Universities (No. 2018CDGFGD0008).

✉ Ben-Jiang Mao
gena@vip.sina.com

1 Department of Engineering Physics, Tsinghua University, Beijing 100084, China

2 Institute of Nuclear Physics and Chemistry, China Academy of Engineering Physics, Mianyang 621999, China

3 Key Laboratory of Optoelectronics Technology and System, Ministry of Education, Chongqing University, Chongqing 400044, China

1 Introduction

A gamma personal dosimeter is a tool for monitoring the radiation dose of workers at a work site, and it is a common and necessary means to ensure the radiation safety of workers at the radiation site [1]. In addition to nuclear power plants and specialized nuclear technology application research institutions, applications of personal dosimeters in the fields of health care, food processing, and industrial manufacturing are very common. Compared to other gamma dosimeters such as portable or area dosimeters, the applications of gamma personal dosimeters are more extensive [2, 3]. In addition, the measured value obtained using a personal dosimeter shows the irradiation dose or dose rate of the wearer, while other gamma dosimeters show the dose rates of the environment.

To ensure measurement accuracy, the ISO-4037 [4–7] series of standards requires periodic calibration of these instruments: a dose-accumulated personal dosimeter should be calibrated twice a year, while a direct-reading personal dosimeter should be calibrated once a year. At present, the calibration work of these instruments should be carried out in a metrological institute with a standard reference radiation (SRR) regulated by relevant standards. According to the ISO-4037 series of standards, the minimum dimensions of an SRR should be not less than $4 \times 4 \times 3\ m^3$. For shielding, i.e., to avoid exposure to gamma rays, a heavy concrete shielding structure must be provided. The large size and heavy weight of the structure make removal inconvenient. Therefore, it can only be calibrated by shipping it to a designated location. The limitation of the traditional calibration method leads to the inability to obtain the staff dose data in time. Sometimes, the staff may even miss the appropriate timing of treatment and health-care measures, and this is very unfavorable to the health protection of staff [8–13].

A feasible solution is to miniaturize the existing calibration device and solve its ray shielding problem so that it can be moved to or near the usual site where the personal dosimeters are widely used for calibration work. In a previous work, Liu [14, 15] first proposed minitype reference radiation (MRR) for the calibration of portable gamma dosimeters. In the experiments, two cubic boxes with lengths 1 m and 0.5 m that were shielded by lead were constructed. A sample-based machine-learning method was applied to determine the conventional true value of air kerma (CAK) at the point of test in MRR successfully with an uncertainty of less than 4.65%. Xu [16] performed simulation to optimize the shielding structure of MRR. Li [17] continued to simulate the distributions of dose rate and scattering spectra in MRR for the purpose of calibrating a portable gamma dosimeter that helps further in optimizing the physical structure of MRR. With the help of the theoretical simulation work, a calibration device for portable gamma dosimeters was developed, and it is shown in Fig. 1.

To expand the function of MRR and make it suitable for the calibration of gamma personal dosimeters, the physical structures of MRR should be reconstructed. Compared with the MRR for the calibration of portable gamma dosimeters, the physical structures of the one used for calibration of personal dosimeters are changed. The changes cause different scattering rays, which affect the reference radiation field. For instance, the mechanical arm applied for grasping the probe should be replaced with a stage for carrying the personal dosimeters. The types and numbers of personal dosimeters are also different from the portable gamma dosimeter to be calibrated in the MRR. When the gamma radiation generated by a Cs-137 source illuminates the personal dosimeters in the shielding box, the inner wall, the personal dosimeters (usually multiple), and the stage inevitably lead to an increase in the scattering ray components in the MRR. This invariably leads to interference in the measurement of the point of test CAK. Therefore, the components of the scattering rays in the MRR for calibration of gamma personal dosimeters are more complicated. The presence of the stage and multiple personal dosimeters increases the scattering rays in the MRR. The point of tests for personal dosimeters is not at the geometric center of the MRR. The angle between the source and the personal dosimeters varies with the shape and model of the personal dosimeters. The scattering rays in the MRR vary with the number of personal dosimeters loaded (to be calibrated). The interferences from the physical structures illustrated above affect the reference radiation field, and this results in different CAKs at the point of test. Therefore, determining the CAK in a different application scenario is crucial for achieving the application of the MRR for the calibration of personal dosimeters.

Fig. 1 (Color online) MRR device for calibration of portable gamma dosimeters

Before developing a CAK determination method at the point of test in MRR for the calibration of personal dosimeters, its characteristics should be studied in detail. In this study, a Monte Carlo simulation investigation was conducted for the MRR to clarify the interferences of different physical structures to the dose field of MRR, and this can help develop a reliable determination method of the CAK at the point of test. By the Monte Carlo method [18], the changes in ray composition, dose rate, and spectrum distribution in the MRR were studied. The results of the study can help to evaluate and verify the determination method of the CAK at the point of test, which is a key technological problem in the application of MRR. Furthermore, this work can benefit the development of the device and facilitate the advancement of MRR-based calibration techniques.

2 Methodology

Based on the existing MRR applied for the calibration of portable gamma dosimeters, the physical model of the one for the calibration of personal dosimeters is reconstructed and shown in Fig. 2. The reference conditions of the MRR are set as follows. (1) The dosimeter size is $5 \times 2 \times 5$ cm^3, and the shell material is plastic. (2) The stage size is $\Phi 30 \times 2$ cm, and the material is polymethyl methacrylate (PMMA). (3) The geometric center of the personal dosimeter is placed 10 cm from the center of the stage. (4) The geometric center of the dosimeter is defined as the point of test of the MRR. This should coincide with the reference point of the personal dosimeter during the

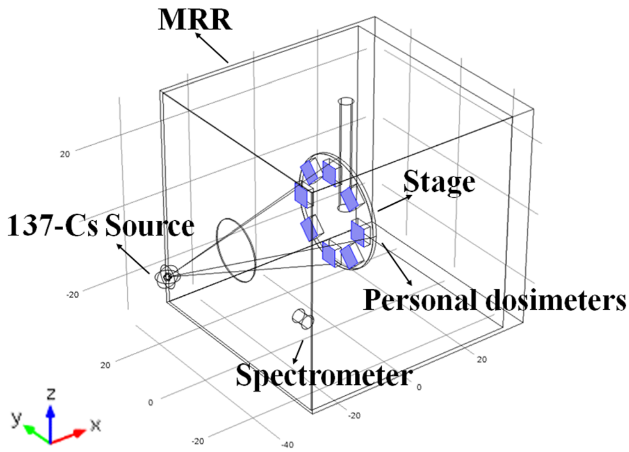

Fig. 2 (Color online) Physical model of MRR for calibration personal dosimeters

calibration work. (5) The Cs-137 source is a point source with an activity of 1 Ci. (6) The ray type is set as a cone beam with a cone angle of 34°, and the cross-sectional diameter of the gamma ray beam at the point of test is 300 mm, which ensures that the eight dosimeters can be completely covered by the beam. (7) The shielding box is made of lead and stainless steel. The inner and outer dimensions of the shielding box are 60 × 60 × 60 cm^3 and 66.3 × 61.6 × 61 cm^3, respectively. The distance between the source and the MRR geometric center is 55 cm.

With the reference condition of the MRR, one can simulate the distributions of the dose rate and gamma spectrum of the radiation field with the changes of different physical structures. Furthermore, the change rules of the MRR can be analyzed in detail for a better understanding of the MRR.

In previous work, the sample-based machine-learning method was applied to determine the CAK in an MRR for the calibration of portable gamma dosimeters. According to the principle of the method, it should additionally be feasible to determine the CAK in an MRR for the calibration of personal dosimeters [19]. In MRR, the air kerma K' measured by a graphite cavity ionization chamber at the point of test without any personal dosimeter placed cannot be treated as the CAK (defined as K below). Because different types and numbers of personal dosimeters are placed in the MRR, the radiation field is affected by different scattering rays. These rays cause a change in K at the point of test. The K cannot be determined directly. Based on the sample-based machine-learning method, common sample dosimeters are selected to acquire sample data applied for training the prediction model of K. A set of sample data included the air kerma values K' and K with sample dosimeters placed at the point of test, and a gamma spectrum S was recorded at the monitoring point in the MRR. To acquire the sample data of K at the point of test in the MRR, a sample dosimeter was applied as a transfer tool to be placed in both the MRR and the SRR. The air kerma at the point in the SRR where the sample dosimeter showed a measured value identical to that measured in the MRR was numerically equal to K. With the sample data acquired, a prediction model of K was trained with the machine-learning method. In a previous study, a least-squares support vector machine method was employed as the machine-learning method [20, 21]. The prediction model of K can be described as Eq. (1).

$$K = f(K', S) \tag{1}$$

With the pretrained prediction model, the K at the point of test in the MRR, when different types and numbers of dosimeters to be calibrated are placed, can be determined indirectly though the measured K' and S. The above description is a brief introduction of the method. The details of every step of the method were presented in Liu's work [14, 15]. The gamma spectrum S plays an important role in predicting the K according to the prediction model. It should effectively characterize the physical structure in MRR. Therefore, the information included in the spectrum should additionally be simulated in this work.

3 Results and discussion

3.1 Uniformity of MRR radiation field

Because of the existence of the stage and several personal dosimeters, the uniformity of the radiation field at the point of test is bound to change. This means that, in the MRR, the composition of the rays that are irradiated onto the dosimeters to be tested is varied. In the absence of a dosimeter to be tested, the dose rate distribution of the gamma ray irradiation direction is as shown in Fig. 3.

The SRR is regulated by the ISO-4037 series of standards, and the dimensions are 4 × 4 × 3 m^3. The medium of the SRR is air. In the SRR, the dose rate values in the radiation field follow the inverse squared attenuation law. Compared with SRR, because the influence of scattering rays in MRR is not negligible, the dose rate of MRR in the direction of gamma ray beam irradiation deviates significantly from the natural attenuation law of gamma rays. The closer to the point of test, the more obvious the deviation. Especially in the vicinity of the stage, because of the interaction of the gamma rays with the stage, the scattering of the stage causes the dose rate of the front surface to be larger, and the absorption of the radiation by the stage causes the dose rate of the rear surface to be less. The rear surface of the shielding box is 85 cm away from the radiation source. Because of the shielding of the lead–steel

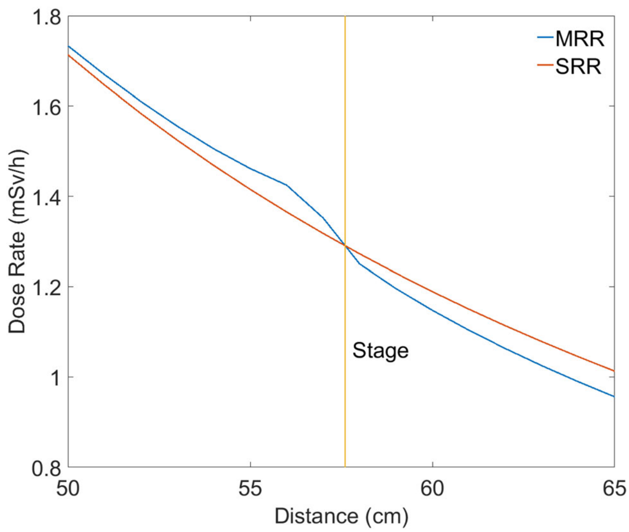

Fig. 3 (Color online) Distribution of dose rate along the irradiation direction

composite material, the dose rate at 5 cm on the outer surface of the device is 2.4 μSv/h lower than the safety limit of 5 μSv/h [4].

In MRR, as the distance increases, the dose rate at the center of the beam decreases continuously, and the trend gradually becomes slower. In the region of 50–60 cm from the radioactive source, the radiation field is affected more significantly. The dose rate at the center of the stage at a distance of 55 cm from the source increases by 3.27%. The closer to the stage, the greater the effect of the dose rate. When the distance source is greater than 65 cm, the dose rate of the beam is less than 1 mSv/h. In actual use, different beam intensities are selected by attenuators on the radiator depending on the different ranges of the dosimeter to be tested. The attenuation range of the radiator is approximately 1–1000 times. The maximum dose rate of the 1 Ci source at the center of the beam at 55 cm from the source can reach 1.5 mSv/h, and the beam intensity varies from 4 to 12 mGy/h. This meets the calibration requirements of radiation protection dosing instruments.

In addition, the number of dosimeters placed is one of the main factors affecting the dose field characteristics of the MRR. Therefore, the distribution of the surface dose rate values of the stage is calculated under the condition of different numbers of dosimeters being placed, and the results are shown in Fig. 4. The serrated edges of the dose section in the figure are caused by the spacing of the simulated points and do not affect the results of the investigation.

When no stage is installed in the MRR, the ray is a cone beam, and a circular high-dose beam spot with a diameter of approximately 30 cm is generated at the center of the point of test, and the relative standard deviation of the intra-area dose rate is approximately 9.98%. When the stage is loaded, the dose value in the central region of the stage changes greatly because of the influence of the scattering of the stage, and the variation range is 2.99%. When a different number of dosimeters are placed on the stage, significant changes in the dose rate distribution at the cross section of the point of test occur. The data in Table 1 give the dose rate at the point of tests when zero, two, four, and eight dosimeters are placed on the stage. The third row is the relative errors of the simulation. As the number of dosimeters is increased, the dose rate at the point of test is increased by 0.56%. This results from the scattering caused by the placed dosimeters; at the same time, the interval between the dosimeters gradually decreases, causing the effects of scattering between them to become more obvious.

3.2 Scattering ray interference at the point of test

The accurate calibration of the dose rate at the point of test in the MRR radiation field is the core problem to be solved in the in situ calibration technology. Therefore, clarifying the scattering rays at the point of test is very important. In particular, because the personal dosimeters are based on different detection principles, the dosimeter shape, size, sensitive volume, and energy response are different too. Here, the dosimeter is simplified into a plastic enclosure for the study of the ray composition and energy at the point of test.

3.2.1 Effect of the stage on the dose rate at the point of test

The calibration of the dosimeter should be performed on the phantom in common. The size and material of the phantom should be such that the sensitive area of the detector in the dosimeter meets the conditions of electronic balance. In the dosimeter applied for measuring $H_p(10)$ on the torso, the dimension of the phantom is $30 \times 30 \times 15$ cm^3, and the wall material is PMMA (the thickness of the front wall material is 2.5 mm, and the other walls are 10 mm). The phantom is filled with water. It is called an "ISO water board phantom". When the average energy of the reference radiation is equal to or higher than 0.662 MeV (Cs-137), a solid PMMA phantom with the same dimensions is applied.

Conventional calibration of dosimeters is not always performed on phantoms. Sometimes, simplified methods work as well, and their validities are preproven [6]. The results obtained by the simplified method are the same as those obtained by standard procedures, or the differences can be reliably corrected. In the MRR, it is impossible to use the ISO phantom because of the limitation of its size. Therefore, the phantom is simplified to a stage composed

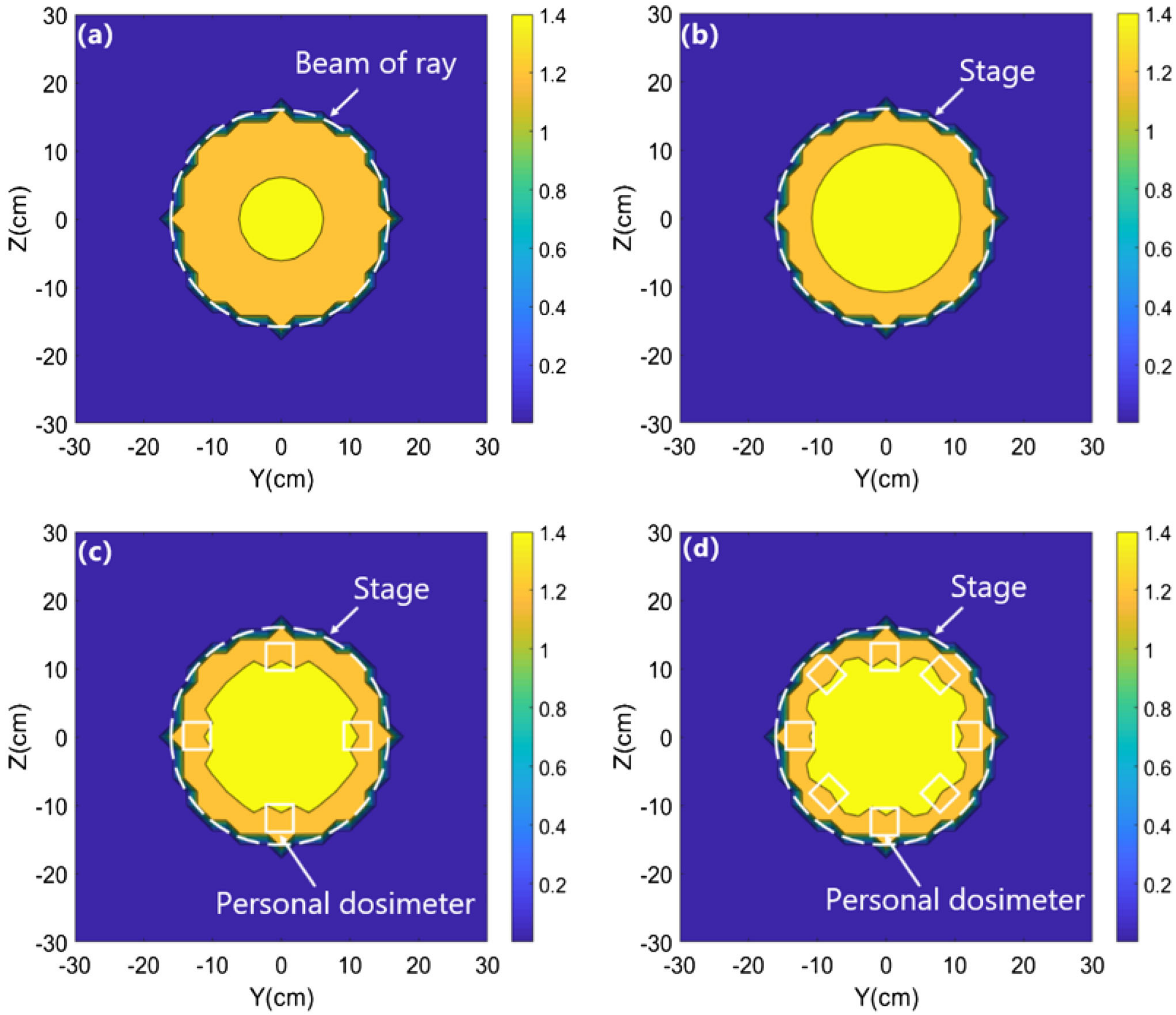

Fig. 4 (Color online) Dose rate distribution at the point of test: **a** without stage and dosimeter, **b** only with stage, **c** with four dosimeters, and **d** with eight dosimeters

Table 1 Dose rates with different numbers of dosimeters at the point of test

Number of dosimeters	Dose rate (mSv/h)	Relative error (%)
0	1.3990	0.5
2	1.4011	0.12
4	1.4023	0.26
8	1.4069	0.2

of a PMMA plate, and the dosimeters are placed on the stage for calibration. In this work, the effects of different thickness stages on the gamma ray composition and energy deposition at the point of test were studied. The gamma energy spectra at the point of test for stages with different thickness loads in the MRR are shown in Fig. 5.

The results show that when stages with different thicknesses are loaded in MRR, there are three scattering characteristic peaks generated around the energies of 0.075, 0.2, and 0.25 MeV in the spectrum. As the thickness of the stage increases, the 0.662 MeV main energy peak and the three scattering characteristic peaks gradually increase, which inevitably leads to an increasing influence of the scattering rays caused by the stage on the dose rate value at the point of test. The ratio of scattering rays to the total energy deposition of incident rays is shown in Table 2.

When the thickness of the stage is 0 mm, there is no stage loaded in the MRR, and the interference of the

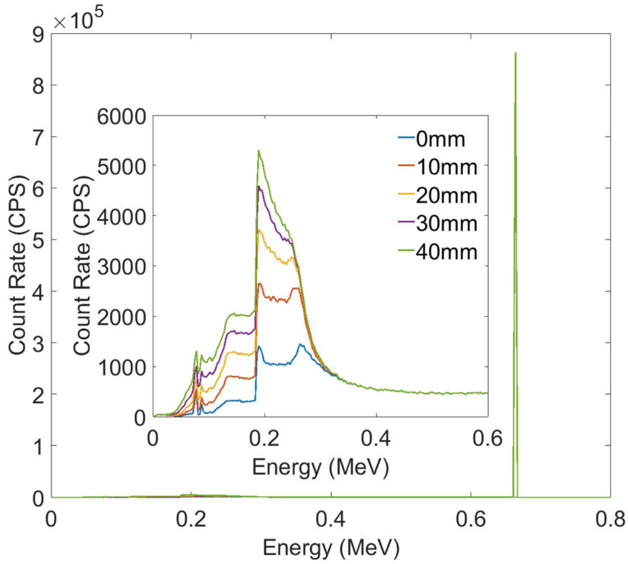

Fig. 5 (Color online) Gamma energy spectrum with different thicknesses of stage at the point of test

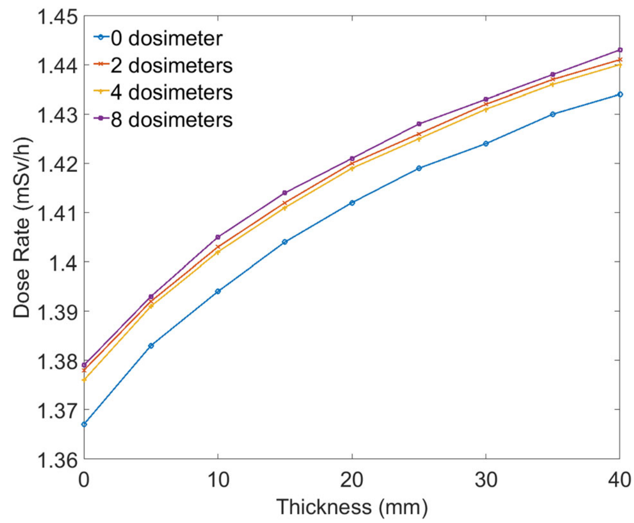

Fig. 6 (Color online) Effect of stage thickness on the dose rate of the point of test

scattering rays is mainly from the inner wall of the MRR. The effect of the change in the thickness of the stage on the dose rate value at the point of test when the stage is placed with a different number of dosimeters is shown in Fig. 6. The influence of the thickness of the stage cannot be neglected. When the thickness of the stage increases, the dose rate value at the point of test gradually increases, while the rate of increase in the dose rate gradually decreases.

Table 3 lists the effect of the thickness of the stage on the dose rate value of the point of test. When the thickness of the stage is not less than 20 mm, the increase rate of the dose rate is reduced to less than 0.50% in every 5 mm increase in the stage thickness, and it gradually becomes stable. At the same time, considering the overall structure of the device, the size of the stage should be as small as possible, so the thickness of the stage is chosen as 20 mm, and the error of insufficient electron balance caused by insufficient thickness of the stage can be controlled within 2%.

Table 3 Impact rate of the stage thickness on the dose rate of the point of test

Thickness of stage (mm)	Influence rate (%)	Relative error (%)
5	1.14	0.11
10	2.00	0.11
15	2.70	0.11
20	3.27	0.11
25	3.78	0.11
30	4.20	0.11
35	4.57	0.09
40	4.90	0.09

3.2.2 *Effect of dosimeter size on the point-of-test dose rate*

According to IEC61526:2010 [22], the maximum size of a personal dosimeter is $15 \times 3 \times 8$ cm^3. The shapes of different types of personal dosimeters are diverse. For the sake of simplicity, cuboids with different scales are selected to characterize the direct-reading personal dosimeters.

Table 2 Ratio of scattering rays to total energy deposition of incident rays

Thickness of stage (mm)	Scattering ray ratio (%)	Relative error (%)
0	11.87	0.33
10	16.18	0.32
20	18.99	0.32
30	21.06	0.32
40	22.63	0.32

The three parameters of length, width, and thickness are changed to investigate the influence of the dosimeter size on the gamma ray composition at the point of test. The gamma energy spectra at the point of test with the size change of the dosimeters are shown in Fig. 7.

When the size of the dosimeter increases, the gamma energy spectrum at the point of test shows an overall growth trend. When the size of the dosimeter is changed, the influences of the gamma spectrum at the point of test are mainly concentrated in the energy range less than 0.3 MeV. The characteristic peaks are generated near the energies of 0.075, 0.2, and 0.25 MeV. When different sizes of dosimeters are introduced, the ratios of scattering rays to the total energy deposition of incident rays are as shown in Table 4.

Table 5 lists the effects of the dosimeter size on the dose rate values of the point of test. The results show that when the thickness of the dosimeter increases, the dose rate at the point of test gradually decreases. This is mainly because the increase in the thickness of the dosimeter has a certain blocking effect on the radiation. With the increase in the side length of the dosimeter, the dose rate at the point of test gradually increases. This phenomenon is mainly because the interval between the dosimeters becomes smaller, so the resulting scatterings are more likely to affect each other.

3.2.3 *Effect of dosimeter number on dose rate at the point of test*

During the calibration work, the number of loaded dosimeters is not always full. Therefore, it is necessary to investigate the effect of the change in dosimeter number on the scattering gamma spectrum at the point of test. When different numbers of dosimeters are loaded in the MRR, the gamma energy spectrum at the point of test is as shown in Fig. 8.

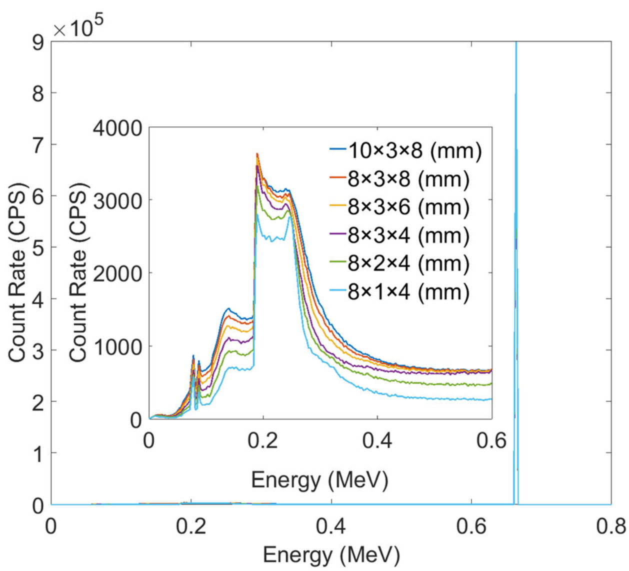

Fig. 7 (Color online) Gamma spectra at the point of test with the size change of dosimeters

In Fig. 8, the positions of the characteristic peaks mainly appear in the vicinity of energies of 0.075, 0.2, and 0.25 MeV. When the number of dosimeters is changed, the change in scattering rays is not significant. The effect of the scattering caused by an increase in the dosimeter number on the point of test dose rate is small, with an influence rate of less than 0.6%. When different numbers of dosimeters are loaded, the ratios of scattering rays to the total energy deposition of incident rays are as shown in Table 6. The effect of the dosimeter number on the point of test dose rate is shown in Table 7.

3.3 Characteristics of the scattering gamma spectrum at the monitoring point

In the MRR applied for the calibration of personal dosimeters, scattering rays are generated by an interaction between the Cs-137 beam and physical structures, including the stage, the inner wall of the shielding box, several dosimeters, and the structure of the shielding box. In the sample-based machine-learning method, the scattering gamma spectrum at the monitoring point is employed to characterize the physical structures of the MRR. The monitoring point was set on the central line of the MRR's inner bottom, near the side of the gamma ray inlet and 100 mm away from the projection point of the point of test. The point has been proven to be the best point for achieving the characteristics in the MRR. When the gamma spectrum at the monitoring point characterizes these rays, rays representing different sources produce characteristic peaks in different energy segments of the monitor spectrum. Therefore, to study the characteristics of scattering rays at the monitoring point, the source of several characteristic peaks should be studied. In the process of simulation, only one specific influencing factor was considered separately. The result is shown in Fig. 9.

There are mainly three characteristic peaks in the monitoring spectrum: 75 keV (peak 1), 200 keV (peak 2), and 240 keV (peak 3). The three factors of the stage, shielding box, and dosimeter have a significant response on the three characteristic peaks.

Characteristic peak 1: This peak is mainly related to the shielding box. Because the energy intensity is less than 0.1 MeV, the peak is the photoelectric effect peak of lead produced by the gamma ray and the lead material of the shield case.

Characteristic peak 2: Reflected in the figure, the characteristic peak is mainly related to the shielding box. The

Table 4 Ratio of scattering rays to total energy deposition of incident rays

Size of dosimeter (mm^3)	Scattering ray ratio (%)	Relative error (%)
10 × 3 × 8	22.45	0.5
8 × 3 × 8	21.79	0.22
8 × 3 × 6	20.84	0.2
8 × 3 × 4	19.50	0.23
8 × 2 × 4	16.75	0.1
8 × 1 × 4	13.06	0.12

Table 5 Impact rate of the dosimeter size on the dose rate of the point of test

Size of dosimeter (mm^3)	Influence rate (%)	Relative error (%)
10 × 3 × 8	1.62	0.03
8 × 3 × 8	1.08	0.04
8 × 3 × 6	0.46	0.04
8 × 3 × 4	− 0.47	0.05
8 × 2 × 4	0.70	0.05
8 × 1 × 4	1.11	0.05

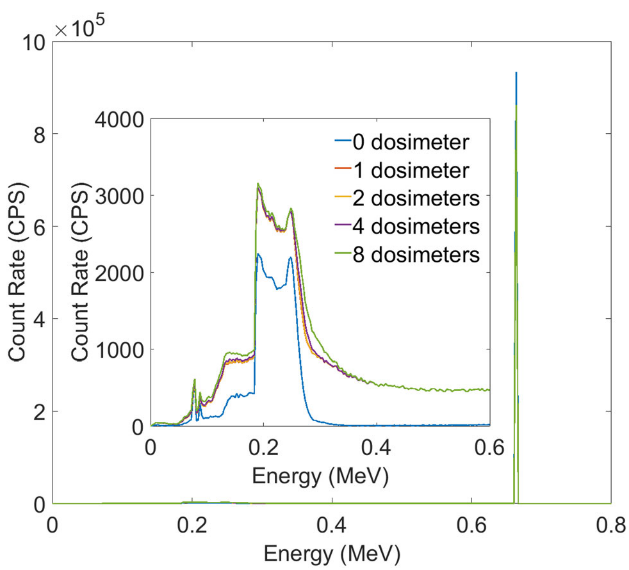

Fig. 8 (Color online) Gamma energy spectrum at the point of test when different numbers of dosimeters are loaded

scattering angle of the rear surface of the shielding box to the monitoring point is approximately 140°. The energy of the corresponding scattering rays is calculated to be 201.3 keV, which is close to the simulated characteristic peak position.

Characteristic peak 3: The gamma ray is irradiated onto the stage and the personal dosimeter, and Compton scattering occurs with a scattering angle of approximately 110°. The calculated scattering corresponding ray energy is 241.7 keV, which is close to the peak energy.

Table 6 Ratio of scattering rays to total energy deposition of incident rays

Number of dosimeters	Scattering ray ratio (%)	Relative error (%)
0	6.29	0.78
1	16.11	0.77
2	16.14	0.76
4	16.31	0.74
8	16.98	0.7

Table 7 Impact rate of the dosimeter number on the dose rate of the point of test

Number of dosimeters	Influence rate (%)	Relative error (%)
1	0.10	0.1
2	0.15	0.09
4	0.24	0.1
8	0.56	0.11

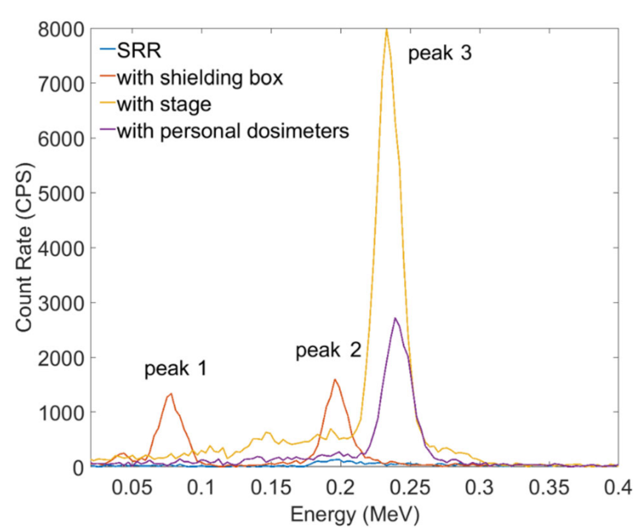

Fig. 9 (Color online) Scattering spectrum at scattering monitor point

The effects of the stage, dosimeter size, and dosimeter number on the scattering spectrum at the scattering monitoring point are shown in Fig. 10.

In practical applications, the thickness of the stage is determined to be constant. However, in the process of designing the device, it is necessary to investigate the influence of the thickness variation of the stage on the scattering energy spectrum of the monitoring point, which ensures that the design of the stage is scientific and reasonable. This indicates that the variation in the thickness of the stage has the most influence on the monitoring point. As the thickness of the stage increases, the effect of the scattering component rises as a whole.

The influence from the personal dosimeter is smaller than that from the stage. When the size and number of the dosimeters increase, the influence on the monitoring point gradually increases, which is manifested in the three characteristic peaks illustrated above. The size and number of dosimeters and the peak value have a positive correlation. This further shows that it is accurate and feasible to characterize the size and number of the dosimeters by monitoring the scattering energy spectrum of the scattering monitoring point.

The scattering spectrum of the monitoring point shows that the conclusions obtained are consistent with the conclusions drawn when calculating the dose rate of the point of test. As the three influencing factors change their respective conditions, the impact on MRR appears to increase or decrease regularly. It is especially important that these causes affecting the MRR gamma ray composition respond to the gamma spectral peaks at the monitoring point. This provides a theoretical basis for accurately

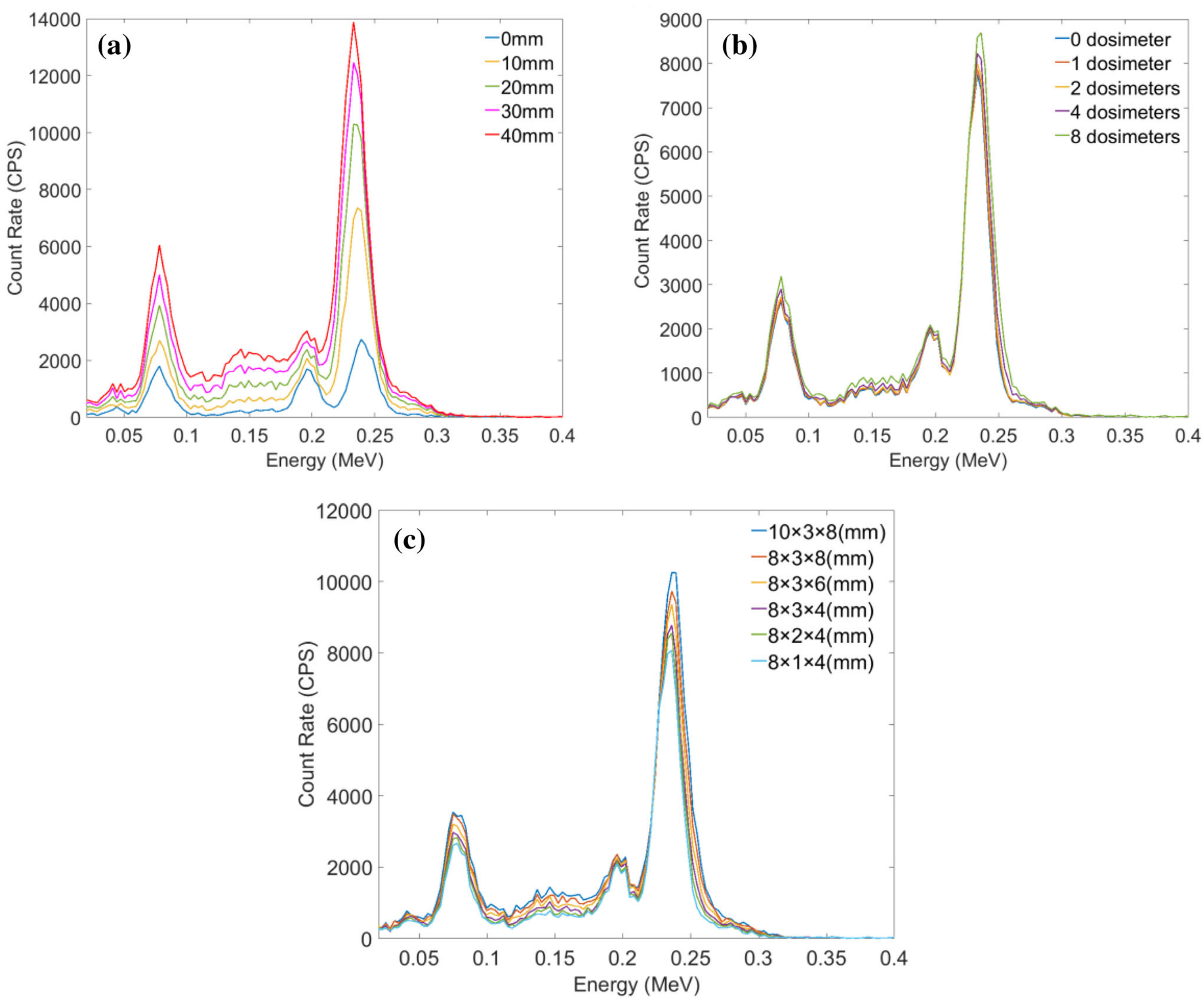

Fig. 10 (Color online) Scattering spectrum at scattering monitoring point under different conditions: **a** stages with different thicknesses, **b** different numbers of dosimeters, and **c** different sizes of dosimeters

reflecting the factors affecting MRR through the energy spectrum of the monitoring point.

4 Conclusion

An MRR physical model was proposed for the calibration of personal dosimeters. A Monte Carlo simulation investigation was carried out to study the characteristics of the radiation field from a Cs-137 radioactive source. The simulation clarified the interferences of the scattering rays from the physical structure of MRR. The results show that the 1 Ci radioactive source (Cs-137) can provide a maximum dose rate of 1.5 mSv/h at the point of test in MRR, thereby meeting the demand of the calibration range of the common personal dosimeters applied for radiation protection. Compared with the MRR applied for the calibration of portable dosimeters, the interference factors of the one for personal dosimeters are raised. According to the simulation and analysis, the interferences of scattering rays from different physical structures are clarified. The simulation results provide references when evaluating the contribution of scattering rays in MRR in future applications. Analyzing the scattering gamma spectrum at the monitoring point shows that the effect on the MRR regularly increases or decreases with the change of each factor; particularly, the thickness of the stage, type of the dosimeter, and the presence of the shielded enclosure. These main factors affecting the MRR gamma ray composition all responded at the gamma spectrum characteristic peak at the monitoring point. This provides a basis or pathway for using the gamma ray spectrum at the monitoring point to characterize the physical structure of the MRR. With the help of these results, an actual experimental device can be constructed to perform the calibration technique for personal dosimeters based on MRR.

References

1. IEC61526, Radiation protection instrumentation-measurement of personal dose equivalents H(10) and H(0,07) for X, gamma, neutron and beta radiations-direct reading personal dose equivalent meters (2010)
2. IEC60846, Radiation protection instrumentation-Ambient and/or directional dose equivalent (rate) meters and/or monitors for beta, X and gamma radiation-part 1: portable workplace and environmental meters and monitors (2009)
3. ISO/IEC Guide 98-3, Uncertainty of measurement-part 3: Guide to the expression of uncertainty in measurement (2008)
4. ISO4037-1, X and gamma reference radiation for calibration dosimeters and dose rate meters and for determining their response as a function of photon energy: I. Radiation characteristics and production methods (1996)
5. ISO4037-2, X and gamma reference radiation for calibration dosimeters and dose rate meters and for determining their response as a function of photon energy: II. Dosimetry for radiation protection over the energy ranges 8 keV to 1.3 MeV and 4 MeV to 9 MeV (1997)
6. ISO4037-3, X and gamma reference radiation for calibration dosimeters and dose rate meters and for determining their response as a function of photo energy: III. Calibration of area and personal dosimeters and the measurement of their response as a function of energy and angle of incidence (1999)
7. ISO4037-4, X and gamma reference radiation for calibration dosimeters and dose rate meters and for determining their response as a function of photo energy: IV. Calibration of area and personal dosimeters in low energy X reference radiation fields (2004)
8. P.J. Lamberti, M. O'brien, *Calibration of X-ray and Gamma Measuring Instruments* (NIST Special Publication, New York, 2001), pp. 250–258. https://doi.org/10.6028/NIST.SP.250-58
9. A. Leitner, J. Witzani, M. Boutillon et al., International comparisons of air kerma standards in ^{137}Cs gamma radiation. Metrologia **34**, 169 (1997). https://doi.org/10.1088/0026-1394/34/2/8
10. C. Kessler, P.J. Allisyroberts, A.V. Oborin et al., Comparison of the standards for air kerma of the VNIIM and the BIPM for ^{137}Cs gamma radiation. Metrologia **47**(1), 6 (2010). https://doi.org/10.1088/0026-1394/47/1A/06007
11. P.J. Allisy-Roberts, C. Kessler, D.T. Burns et al., Comparisons of the standards for air kerma of the GUM and the BIPM for ^{60}Co and ^{137}Cs gamma radiation. Metrologia **48**(1A), 6015-06015 (2011). https://doi.org/10.1088/0026-1394/48/1A/06015
12. C. Kessler, P.J. Allisy Roberts, D.T. Burns et al., Comparison of the standards for air kerma of the ITN (Portugal) and the BIPM for 137cs γ-rays. Metrologia **47**(1A), 06007 (2009). https://doi.org/10.1088/0026-1394/47/1A/06022
13. C. Kessler, P.J. Allisy Roberts, A. Steurer et al., Key comparison: comparison of the standards for air kerma of the BEV and the BIMP for 60co gamma radiation. Metrologia **50**(1A), 06002 (2011). https://doi.org/10.1088/0026-1394/50/1A/06002
14. Y.X. Liu, B. Wei, R.H. Zhuo et al., Determination of the conventional true value of gamma air kerma in a minitype reference radiation. Appl. Radiat. Isotopes **118**, 238 (2016). https://doi.org/10.1016/j.apradiso.2016.09.018
15. Y.X. Liu, B. Wei, Y. Xu et al., Feasibility study on determining the conventional true value of gamma air kerma in a minitype reference radiation. Nucl. Sci. Tech. **28**, 80 (2017). https://doi.org/10.1016/j.apradiso.2016.09.018
16. Y. Xu, B. Wei, B.J. Mao et al., Shielding research of minitype reference radiation device based on Monte Carlo simulation. High Power Laser Part. Beams **28**, 168–175 (2016). https://doi.org/10.11884/HPLPB201628.160018
17. W.J. Li, Y.X. Liu, B. Wei et al., Monte Carlo simulation investigation on the minitype reference radiation employed for the calibration on gamma ray dose or dose rate meters. J. Radiol. Prot. **38**, 407–421 (2018). https://doi.org/10.1088/1361-6498/aa9fb9
18. MCNP3B, Monte Carlo Neutron and Photo Transport Code System, ccc-200 (1989)
19. L.J. Cao, K.S. Chua, W.K. Chong et al., A comparison of PCA, KPCA and ICA for dimensionality reduction in support vector machine. Neurocomputing **55**(1), 321–336 (2003). https://doi.org/10.1016/s0925-2312(03)00433-8
20. K. Pelckmans, J.A.K. Suykens, LS-SVMlab Toolbox User's Guide, Katholieke Universiteit Leuven, ESAT-SCD-SISTA Technical Report, 02-145 (2003)

21. N. Cristianini, J. Shawe Taylor, *An Introduction to Support Vector Machines and Other Kernel Based Learning Methods* (Cambridge University Press, Cambridge, 2000)

22. IEC61526, Radiation protection instrumentation-measurement of personal dose equivalents Hp(10) and Hp(0.07) for X, gamma, neutron and beta radiations-direct reading personal dose equivalent meters (2010)